Supporting Information

Influence of Blend Morphology and Energetics on Charge Separation and Recombination Dynamics in Organic Solar Cells incorporating a Non-Fullerene Acceptor

*Hyojung Cha, Scot Wheeler, Sarah Holliday, Stoichko Dimitrov, Andrew Wadsworth, Hyun Hwi Lee, Derya Baran, Iain McCulloch, and James R. Durrant**

Figure S10. Excitation fluence dependence of the non-geminate recombination dynamics (0.5 -6 ns) in (a) PffBT4T-2OD:$PC_{71}BM$ and (b) PffBT4T-2OD:FBR blend films excited at 715nm.

Figure S11. (a) Langerin reduction factor from measured bimolecular recombination rate which is obtained from TPV and CE at open circuit, and (b) ideality factors as a function of voltage of PffBT4T-2OD-based blend solar cells.

Figure S12. Total charge (Q_{tot}) as a function of delay time (t_d) for different values of the prebias for PffBT4T-2OD:FBR device.

FBR : (Z)-5-{[5-(7-{5-[(Z)-(3-Ethyl-4-oxo-2-thioxo-1,3-thiazolidin-5-ylidene)methyl]-8-thia-7.9-diazabicyclo[4.3.0]nona-1(9),2,4,6-tetraen-2-yl}-9,9-dioctyl-9H-fluoren-2-yl)-8-thia-7.9-diazabicyclo[4.3.0]nona-1(9),2,4,6-tetraen-2-yl]methylidene}-3-ethyl-2-thioxo-1,3-thiazolidin-4-one.

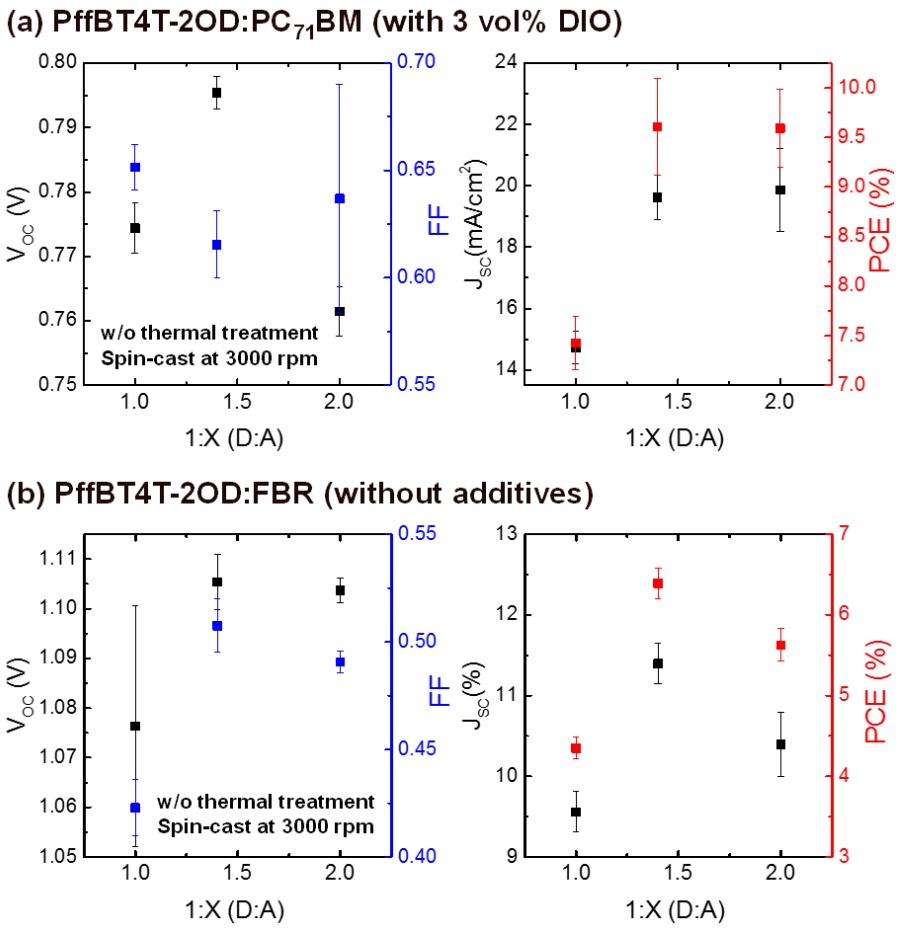

Figure S1. Device performance with various ratios of donor:acceptor: (a) PffBT4T-2OD:$PC_{71}BM$ blend films with 3 vol% of DIO, and (b) PffBT4T-2OD:FBR blend films without using processing additives.

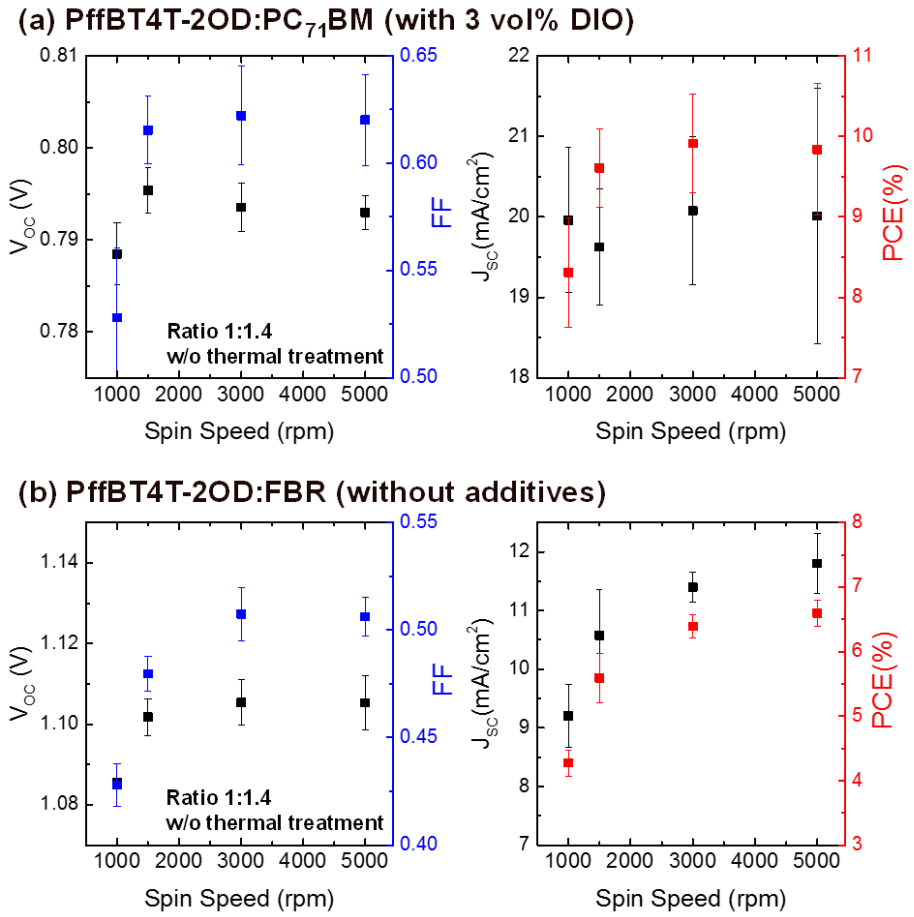

Figure S2. Device performance with various spin speeds while donor:acceptor films are fabricated: (a) PffBT4T-2OD:$PC_{71}BM$ blend films with 3 vol% of DIO, and (b) PffBT4T-2OD:FBR blend films without using processing additives.

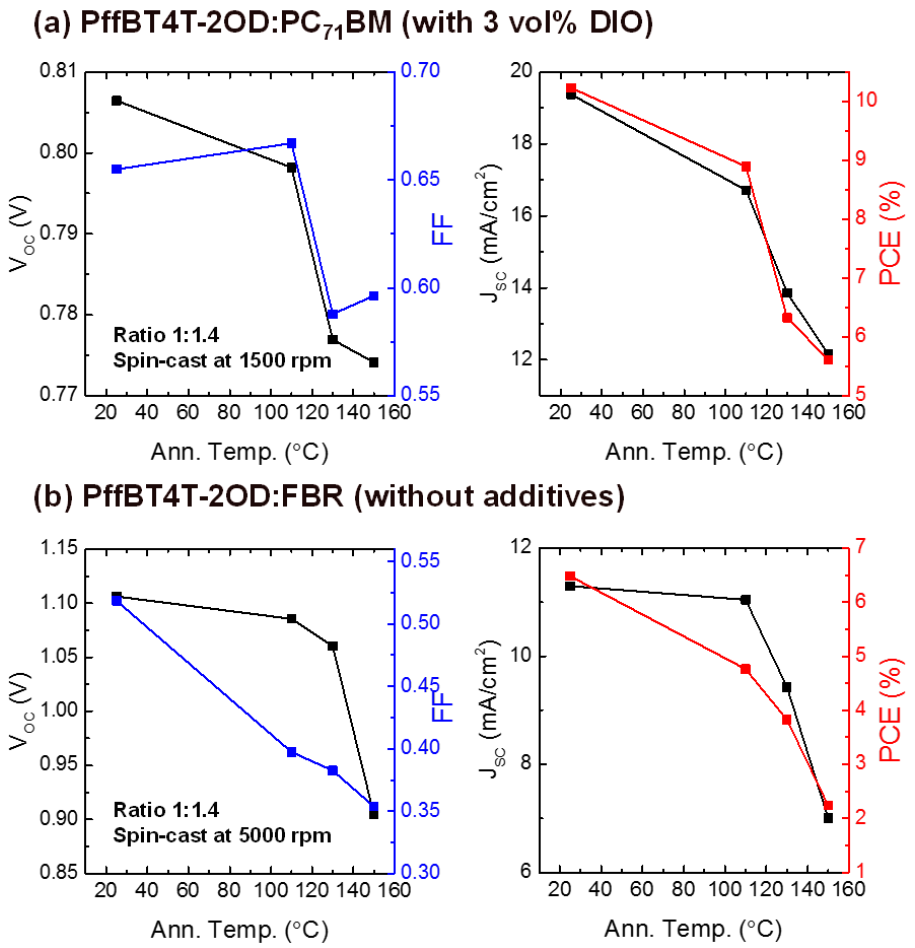

Figure S3. Device performance with various annealing temperatures of donor:acceptor blend films: (a) PffBT4T-2OD:$PC_{71}BM$ with 3 vol% of DIO, and (b) PffBT4T-2OD:FBR without using processing additives.

Figure S4. J_{SC} as a function of light intensity for PffBT4T-2OD:$PC_{71}BM$ and PffBT4T-2OD:FBR (b) linearity of J_{SC} for both systems calculated from the gradient of (a) $dJ_{SC}/d\phi$.

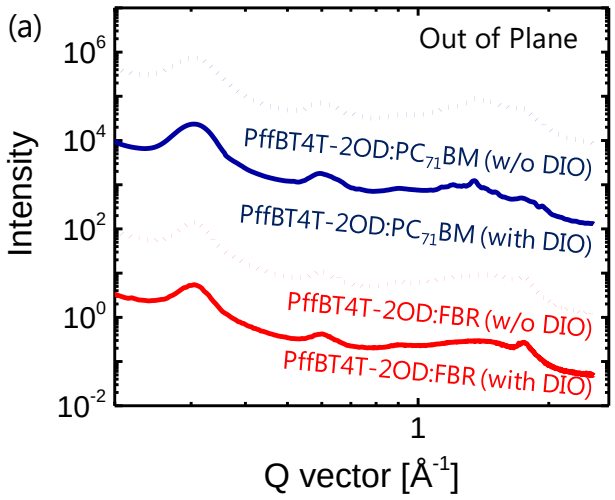

Figure S5. GIWAXS data in the out-of-plane direction of PffBT4T-2OD:PC_{71}BM films and PffBT4T-2OD:FBR films without additive and with 3vol% of DIO.

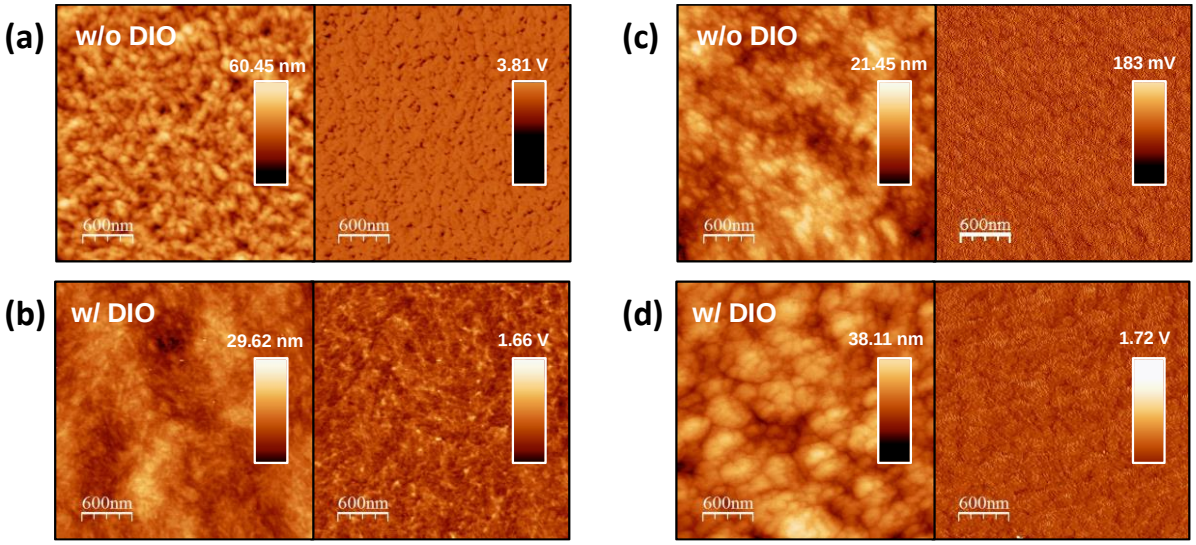

Figure S6. AFM images (3 μm×3 μm) of (a) PffBT4T-2OD:$PC_{71}BM$ films and (b) PffBT4T-2OD:FBR films processed with and without 3 vol% of DIO. Height mode images (left) and phase mode images (right).

Calculation of exciton diffusion lengths by using modified singlet−singlet exciton annihilation (EEA): femtosecond-transient absorption data of neat PffBT4T-2OD films excited with the various excitation intensities was used to calculate diffusion length of the polymer excitons. In this EEA method[23,24], exciton quenchers, which may disturb blend morphology, are not necessary. The model used, assumes that exciton decay via radiative and non-radiative deactivations with intrinsic exciton lifetime constant (k) and via bimolecular EEA with a bimolecular decay rate coefficient (γ), as shown in Equation S2, where $n(t)$, in cm^{-3} is the exciton density at a delay time t after the laser excitation,

$$-\frac{dn(t)}{dt} = kn + \gamma n^2 \qquad \text{(Eq. S2)}$$

$$n(t) = \frac{n_0 \exp(-kt)}{1+(\gamma/k)n_0[1-\exp(-kt)]} \qquad \text{(Eq. S3)}$$

A useful indication of the rate of a first-order chemical reaction is the half-life, $t_{1/2}$, of total photo-induced exciton, the time taken for the concentration of exciton to decay to half its initial value. Our modification to the methodology proposed by Samuel and collaborators[23] consists in determining the EEA coefficient by comparing the half-lifetime of transients at low excitation intensity, where we assume that EEA is completely absent and at high excitation intensities, where EEA takes place. The time for $n(t)$ to decrease from n_0 to $\frac{1}{2}n_0$ in a first-order reaction is given by

$$t_{1/2} = t_0 = \frac{\ln 2}{k} \qquad \text{(Eq. S4)}$$

The main point to note about this result is that, for a first-order reaction, the half-life of total photo-induced exciton is independent of its initial concentration. Therefore, if the concentration of exciton at some arbitrary stage of the reaction is $n(t)$, then it will have decayed to $\frac{1}{2}n_0$ after a further interval of $\frac{\ln 2}{k}$. To combine first-order reaction and second-order reaction, we take two different excitation densities. At low excitation density, $t_{1/2}$ put the initial time t_0, and should be $t_0 = \frac{\ln 2}{k}$ with first-order reaction. On the other hand, at high excitation density, $t_{1/2} = 2t_0 = \frac{\alpha \ln 2}{k}$, when $\alpha < 1$.

We can then rearrange this expression (Eq. S3) with the half-life of exciton decay,

$$\frac{n(t)}{n_0} = \frac{\exp(-kt_{1/2})}{1+(\gamma/k)n_0[1-\exp(-kt_{1/2})]} = \frac{1}{2} \quad \text{at } t=t_{1/2} \qquad \text{(Eq. S5)}$$

It follows that

$$\exp(-kt_{1/2}) = \frac{1+\frac{\gamma}{k}n_0}{2+\frac{\gamma}{k}n_0} \quad \text{(Eq. S6)}$$

By substituting $t_{1/2} = \frac{\alpha \ln 2}{k}$,

$$\gamma = \frac{k(2\exp(-\alpha \ln 2)-1)}{n_0(1-\exp(-\alpha \ln 2))} \quad \text{(Eq. S7)}$$

If the α is low enough, $\exp(-\alpha \ln 2) = 1 - \alpha \ln 2$

Hence

$$\gamma = \frac{k(2-2\alpha \ln 2-1)}{n_0 \alpha \ln 2} = \frac{k}{n_0 \alpha \ln 2} = \frac{1}{n_0 t_{1/2}} \quad \text{(Eq. S8)}$$

Unlike a first-order reaction, the half-life of exciton decay in a second-order reaction varies with the initial concentration. A practical consequence of this dependence is that species that decay by second-order reactions may persist in low concentrations for long periods because their half-lives are long when their concentrations are low.

The modified EEA bimolecular decay rate coefficient was obtained from (eq. S7) and was calculated to be to be $\gamma = 9.63\times10^{-9}$ $cm^3 s^{-1}$ at excitation fluence of 10 μJ/cm^2.

$$\gamma = 4\pi R_a D \quad \text{(Eq. S9)}$$

The exciton diffusion coefficient (D) is determined using bimolecular decay rate coefficient is determined shown in Equation S9. Once the EEA coefficient is determined, the diffusivity constant D is determined using Equation S5, and considering an annihilation radius of excitons to be mainly driven by dipole-dipole interactions. To estimate, the π-π stacking distance was considered to be the average exciton hopping distance[23,24], and correspond to the Förster radii for exciton transfer onto an excited and a ground state segment of the polymer respectively[23,24]. We used an upper estimate of ⁄ to get an annihilation radius. We used an annihilation radius R_a = 2.88 nm corresponds to the distance in which singlet-singlet exciton annihilation is faster than diffusion. D = 2.66×10^{-3} cm^2s^{-1} was obtained by using Equation S9. The exciton diffusion length (L_d) of 10.9 nm can be calculated using,

$$L_d = \sqrt{D \cdot \tau} \quad \text{(Eq. S10)}$$

In identical method, the diffusion coefficient and diffusion length of FBR is D = 5.84×10^{-3} cm^2s^{-1} and 5.4 nm.

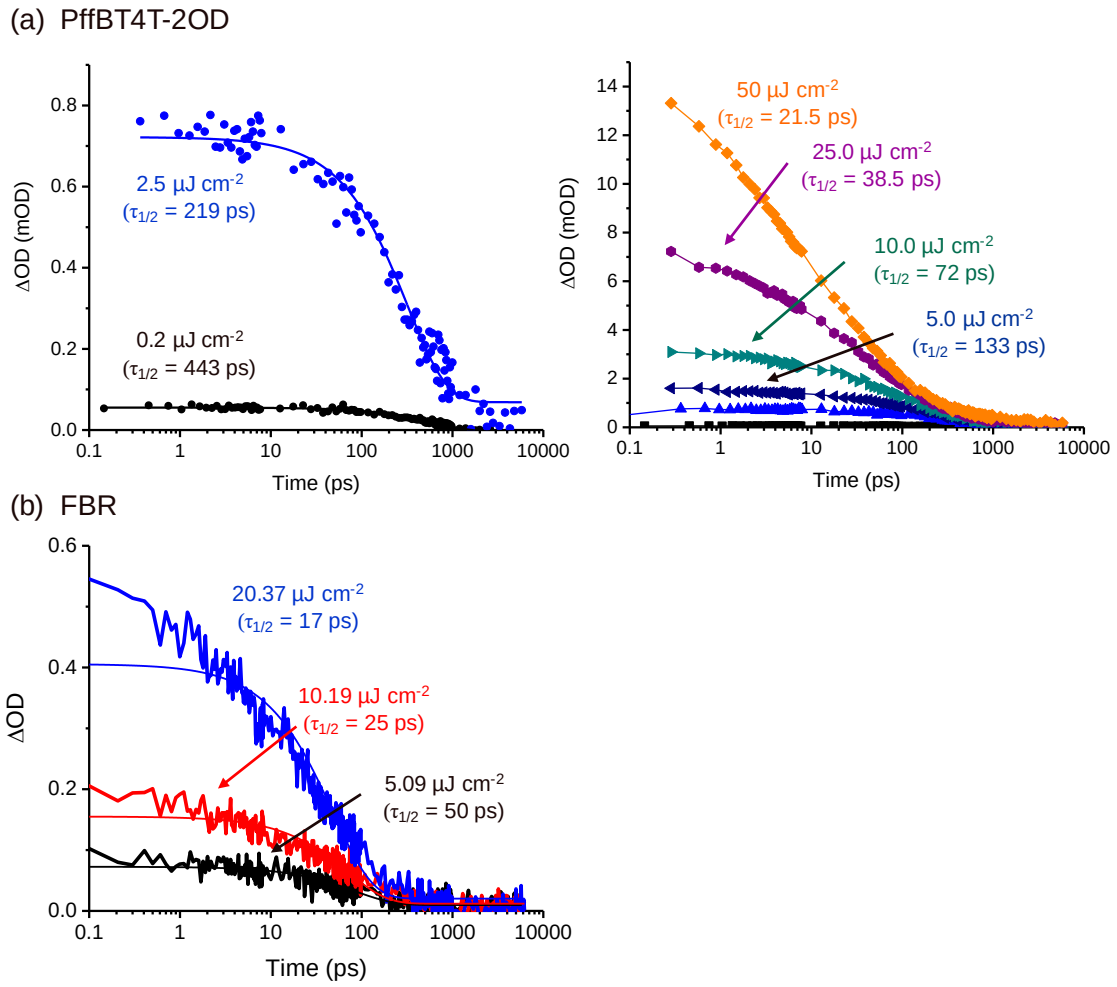

Figure S7. Single exciton decay dynamic for (a) PffBT4T-2OD excited at 715 nm and (b) FBR excited at 530nm with various excitation fluence.

Table S1. Parametres of single exciton decay dynamic for neat PffBT4T-2OD films excited at 715 nm.

Energy μJ cm^{-2}	**n_0 ×10^{17}**	**$t_{1/2}$ ps**	***k* ×10^9**	**α**	**γ ×10^{-9} cm^3 s^{-1}**	***D* ×10 cm^{2}s^{-1}**	**L_d nm**
0.2	0.24	443	1.56				
2.5	3.00	219		0.49	7.55	2.09	9.61
5	6.00	133		0.30	8.66	2.39	10.30
10	12.0	72		0.16	9.63	2.66	10.86
25	30.0	38.5		0.087	7.88	2.18	9.82
50	60.0	21.5		0.049	7.36	2.03	9.49

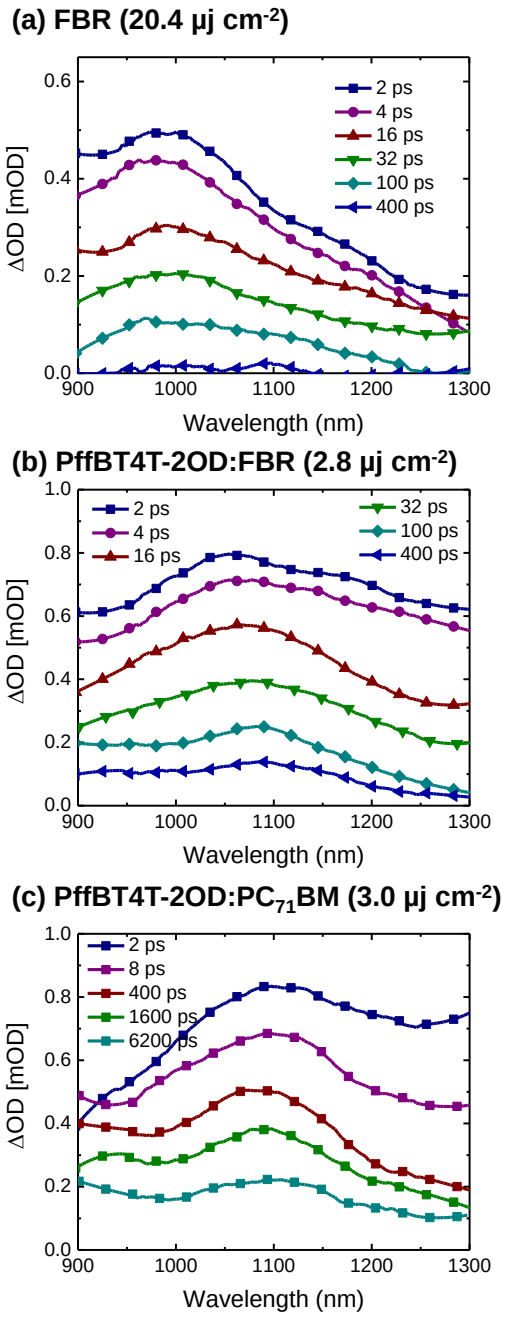

Figure S8. The fs-transient absorption spectra of (a) neat FBR film, (b) PffBT4T-2OD:$PC_{71}BM$ blend film, and (c) PffBT4T-2OD:FBR blend film excited at 530 nm.

The decay dynamics of charge carriers originating from the FBR singlet exciton are investigated with fs-TAS using an excitation wavelength of 530 nm, corresponding to the maximum absorption of FBR. Figure S8 exhibits the typical transient absorption spectra of neat FBR, and the blend films on 200 fs–6 ns time scales. For PffBT4T-2OD:FBR blend films, the transient absorption spectra at early times exhibit a broad signal in the range of 900–1300 nm which overlapped by singlet exciton signals of neat polymer and neat FBR as well as

long-lived polaron states, however, photoinduced absorption spectrum of PffBT4T-2OD:$PC_{71}BM$ show similar behaviour to those excited on polymer at 715 nm without photoinduced absorption at 900 nm. A residual shoulder at 1100 nm is increasingly apparent at long times and assigned to a yield of long-lived polaron states in both blend films and photoinduced charge separation from FBR singlet excitons. Figure S8c compares the FBR exciton decay dynamics, monitored at the exciton photoinduced absorption maximum of 1100 nm. At early times, observed exciton decay signal of PffBT4T-2OD:$PC_{71}BM$ blend excited at 530 nm is similar to that excited at 715 nm, assigned to singlet exciton decay from PffBT4T-2OD. In contrast, the photoinduced exciton decay time in PffBT4T-2OD:FBR rises at early time, contributed to the high exciton density caused by exciton generation of FBR. At longer times, PffBT4T-2OD:FBR blend film shows rather fast geminate recombination dynamics and less long-lived polaron pairs compared to PffBT4T-2OD:$PC_{71}BM$ blend.

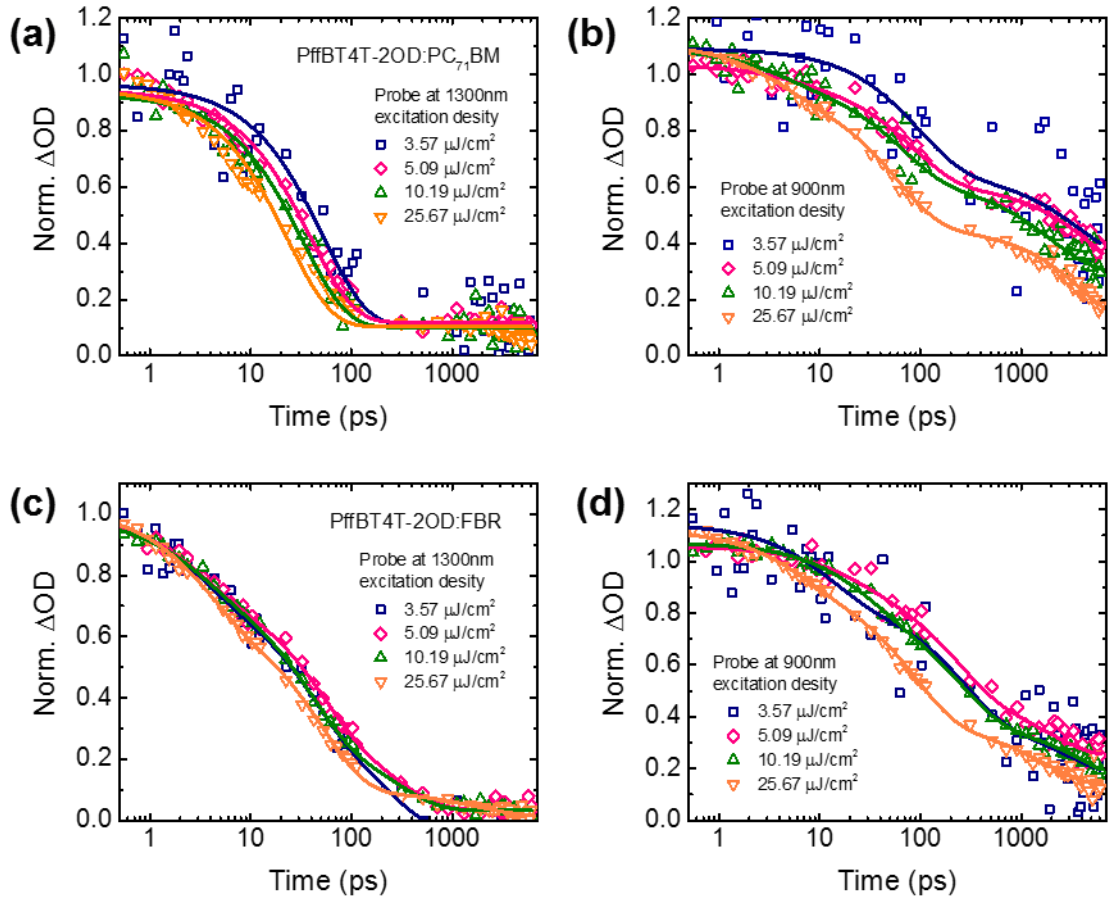

Figure S9. Excitation fluence dependence of the recombination dynamics in (a-b) PffBT4T-2OD:$PC_{71}BM$ blend films, and (c-d) PffBT4T-2OD:FBR blend films excited at 715 nm.

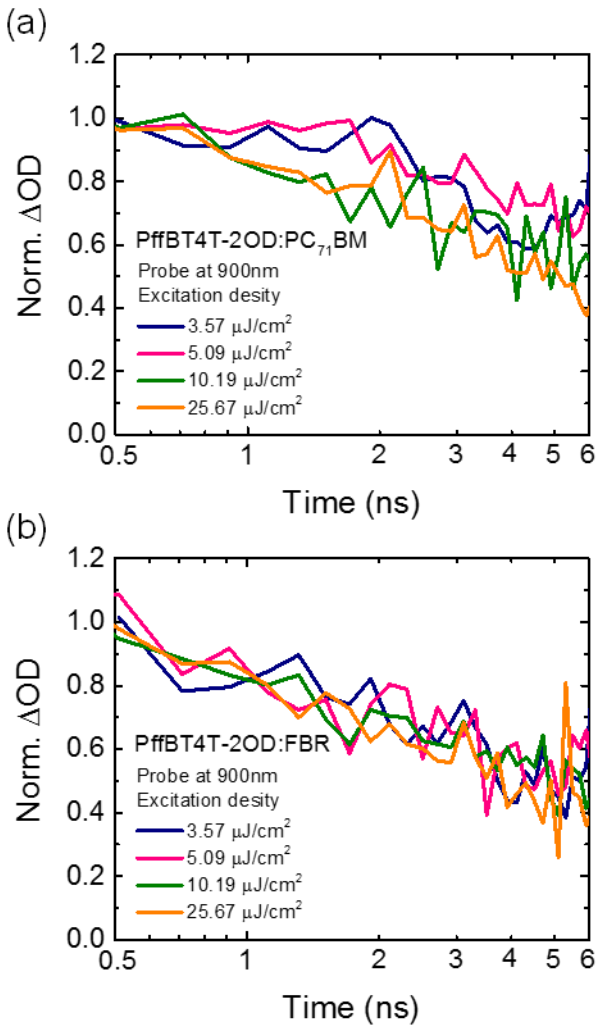

Figure S10. Excitation fluence dependence of the non-geminate recombination dynamics (0.5 -6 ns) in (a) PffBT4T-2OD:$PC_{71}BM$ and (b) PffBT4T-2OD:FBR blend films excited at 715nm.

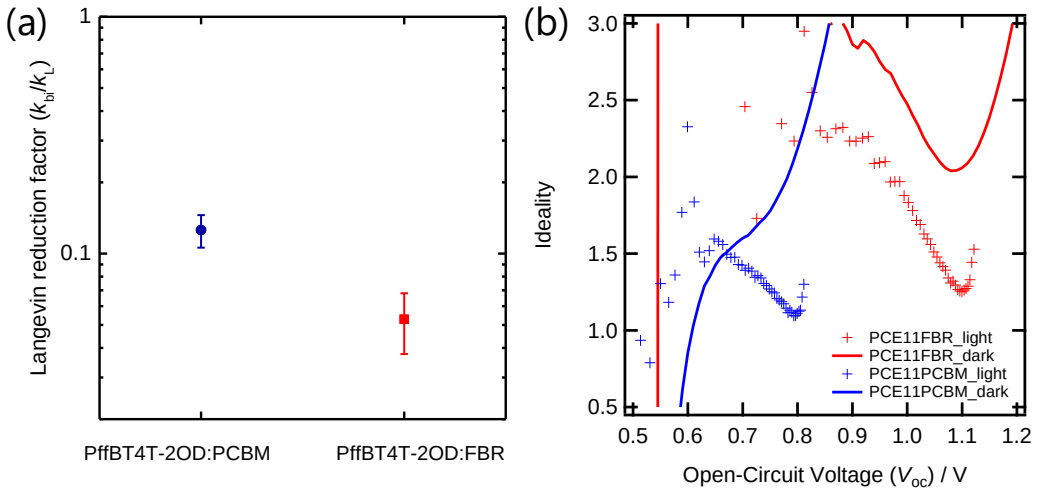

Figure S11. (a) Langerin reduction factor from measured bimolecular recombination rate which is obtained from TPV and CE at open circuit, and (b) ideality factors as a function of voltage of PffBT4T-2OD-based blend solar cells.

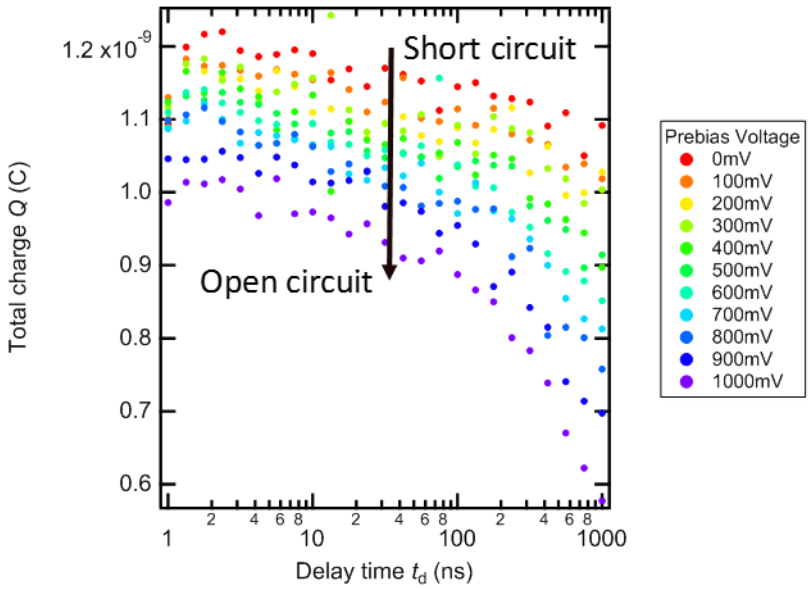

Figure S12. Total charge (Q_{tot}) as a function of delay time (t_d) for different values of the prebias for PffBT4T-2OD:FBR device.